Polymer Chemistry

ROYAL SOCIETY OF CHEMISTRY

PAPER

View Article Online
View Journal | View Issue

Cite this: *Polym. Chem.*, 2024, **15**, 2070

Solvent effects on surface-grafted and solution-born poly[*N*-(2-hydroxypropyl)methacrylamide] during surface-initiated RAFT polymerization†

Yu-Min Wang, *[a] Anna Kálosi,[b,c] Yuriy Halahovets,[c] Hynek Beneš, [a] Andres de los Santos Pereira [a] and Ognen Pop-Georgievski *[a]

Received 16th February 2024,
Accepted 24th April 2024

DOI: 10.1039/d4py00177j

rsc.li/polymers

The difference in the molar mass between surface-grafted and solution-born polymers grown during surface-initiated (SI) polymerization has caused controversy for years. To understand it, we study the solvent effects on the polymer formed on the surface and in the solution by investigating their macromolecular parameters. We utilized reversible addition fragmentation chain-transfer (RAFT) polymerization to grow surface-grafted and solution-born poly[*N*-(2-hydroxypropyl)methacrylamide] (p(HPMA)) under different solvent conditions. Changing the solvent proticity and/or polarity influences the solution propagation rate, leading to mass transfer limitations and a concomitant discrepancy in the molar masses of the polymer formed in solution and grafted from the surface. Moreover, the solvent effects were found to directly determine the grafting density of surface-grafted p(HPMA). These results highlight how decisive the solvent effects on the SI-RAFT polymerization of HPMA are and that they may be key to regulate the physical and macromolecular parameters of the obtained surface-grafted p(HPMA) brushes.

Introduction

Poly[*N*-(2-hydroxypropyl)methacrylamide] (p(HPMA)) represents the state of the art of biocompatible, non-toxic, and non-immunogenic polymers and has found extensive use in drug delivery.[1–4] Its polymer brush coatings on surfaces inhibit non-specific protein binding (fouling) in various biomedical applications.[5–8] P(HPMA) brushes showed outstanding hemocompatibility and prevented surface thrombogenicity under dynamic flow conditions.[6,9] In our previous study,[10] we reported that the antifouling performance of the p(HPMA) brushes increased with increasing grafting density of the polymer chains. Importantly, we showed how the selection of the grafting method directly affects the grafting density of the p(HPMA) coatings on the surface and that denser polymer brushes can be achieved by the grafting-from (GF) approach. Methods employed for GF typically rely on controlled radical polymerizations (CRP),[11,12] such as nitroxide-mediated polymerization,[13–15] atom-transfer radical polymerization (ATRP)[16–21] and reversible addition fragmentation chain-transfer (RAFT) polymerization.[22–28] In particular, surface-initiated (SI) RAFT polymerization is gaining increased attention due to its advantageous features, such as excellent monomer compatibility and lack of metal catalysts toxic to cells, which is beneficial for biomaterial applications.[29–31]

Besides the grafting density of the polymer brush, the molar mass of the polymer chains on the surface is also an important physical parameter influencing the coating's antifouling ability[32] but it is challenging to measure it directly.[33–35] The difficulty in accessing the molar mass distribution of surface-grafted polymer generated during SI polymerizations comes from the fact that its mass is extremely low, making analysis by typical methods such as size-exclusion chromatography (SEC) problematic. While some authors have assumed that the molar mass of the surface-grafted polymer is comparable with that of the polymer grown concomitantly in solution during the SI-polymerization,[36] experimental studies have demonstrated that the polymer molar mass on the surface and the solution-born polymers may be similar or differ greatly, depending on polymerization conditions.[37–39] Genzer's and Spencer's groups attributed this discrepancy to a phenomenon they termed "crowding" during SI-ATRP polymerization at high grafting density and/or with a high propagation rate.[40,41] Crowding limits mass transfer at the surface, slowing down

[a]*Institute of Macromolecular Chemistry, Czech Academy of Sciences, Heyrovského nám. 2, 16200 Prague, Czech Republic. E-mail: yumin810229@gmail.com, georgievski@imc.cas.cz*
[b]*Centre for Advanced Materials Application, Slovak Academy of Sciences, Dúbravská cesta 9, 84511 Bratislava, Slovakia*
[c]*Department of Multilayers and Nanostructures, Institute of Physics, Slovak Academy of Sciences, Dúbravská cesta 9, 84511 Bratislava, Slovakia*

† Electronic supplementary information (ESI) available. See DOI: https://doi.org/10.1039/d4py00177j

the propagation rate in comparison to that in the solution. However, it remains an open question to which extent such effect is present in SI-RAFT polymerization and which factors may influence it. This is crucial to optimize the GF-method using SI-RAFT polymerization.

In order to study the SI-RAFT polymerization kinetics of the surface-grafted polymer, the group of Prof. Barner-Kowollik introduced single-molecule force spectroscopy (SMFS) as a powerful method.[33] This technique harnesses the sensitivity of atomic force microscopy (AFM) to record force–distance curves as individual surface-grafted polymer chains are bound to the tip and extended during tip retraction to extract their contour length.[42] To ensure that the whole contour length of the polymer is accessed during measurement, the chains must be bound to the AFM tip by their end group.[33] For this purpose, after SI-RAFT polymerization the terminal chain transfer agent group capping the chains can be conveniently converted to thiol, allowing for chemical bonding between polymer chain and a gold-coated AFM tip.[10,26,43] Thus, SMFS offers a practical and effective approach for characterizing the molar mass distribution of surface-grafted polymer brushes.[33,44,45] Brooks and colleagues conducted a comprehensive evaluation of SMFS on polymer brushes that had varying grafting densities and showed excellent agreement between the molar masses obtained by SMFS and by SEC from de-grafted polymer chains.[35] Several studies demonstrated the reliability of AFM and AFM-SMFS, establishing them as powerful alternatives for the molar mass determination of molecular brushes and surface-grafted polymer chains, which can bypass the difficulties of traditional methods.[35,46–48]

The choice of solvent plays a crucial role in the mechanism of CRP including their solution and surface-initiated polymerizations. Solvent effects can differently affect the propagation rate of various monomers.[49] They are also critical when the solvent molecules determine the interactions between polymer chains or directly interact with them, for example in polyzwitterionic brushes.[50,51] Moreover, in ATRP the solvent polarity affects the reaction kinetics by influencing the rates of activation and deactivation and the ATRP equilibrium constant.[37,52,53] Similarly, in RAFT polymerization the solvent composition can influence the fragmentation rate of the RAFT agent-radical adduct and impact the attainable control and conversion, as shown by Thang and co-workers specifically for the RAFT polymerization of HPMA in solution.[54,55] However, the effects of solvent composition on the SI-RAFT polymerization for the grafting of p(HPMA) brushes remain unexplored, even though such brushes are of great interest due to their excellent fouling resistance.

In the current study, we investigate the differences between surface-grafted and solution-born polymer during the RAFT polymerization of HPMA by manipulating the solvent composition. We characterize the conversion and molecular weight distribution in solution by NMR spectroscopy and SEC and assess the concomitant growth of surface-grafted p(HPMA) brushes by spectroscopic ellipsometry and SMFS. Additionally, we measured the dynamic viscosity of the polymerization solutions and its shear-rate dependence to address the possible mass transfer limitations occurring during the SI-RAFT polymerization, due to the effect of viscosity on diffusion. By leveraging solvent effects, we verify a discrepancy between surface-grafted and solution-born polymers in the context of SI-RAFT polymerization. The influence of solvent composition on the surface-grafted polymer is revealed to be complex and act by various simultaneous mechanisms, affecting propagation rate, mass transport and grafting density.

Experimental section

Materials

Silicon wafers (orientation ⟨100⟩) bearing native silicon oxide layer were purchased from Siegert Wafer GmbH (Germany). Copper(I) bromide (CuBr, 99.99%), 2,2′-bipyridyl (BiPy, 99%), 4-cyano-4-(phenylcarbonothioylthio) pentanoic acid (CTA), 2,2′-azobis(2-methylpropionitrile) (AIBN), triethylamine (TEA, 99.5%) and hexylamine (99%) were purchased from Sigma-Aldrich (Czech Republic). TEA was purified by distillation over CaH_2 before use. All other reagents were used as received. Dimethyl sulfoxide (DMSO), dimethylformamide (DMF), 1,4-dioxane and toluene were purchased from Acros Organics (extra dry, kept over molecular sieves, and filtered using 0.22 μm syringe filter before use). The other organic solvents of analytical grade were from Lach-Ner (Czech Republic) at the highest available purity and used as received. Deionized (DI) water was obtained from a Milli-Q purification system (Milli-Q gradient A10, Merck-Millipore). [11-(2-Bromo-2-methyl)-propionyloxy]undecyltrichlorosilane (Br-silane) and *N*-(2-hydroxypropyl)methacrylamide (HPMA) were synthesized according to the procedures reported earlier.[56,57]

Synthesis

Self-assembled monolayer on the substrates and CTA immobilization. First, the silicon substrates were cleaned by rinsing with ethanol and DI water twice, dried under a stream of nitrogen, and then activated in a UV/O_3 cleaner for 20 min. Immediately, they were immersed in a 0.1% v/v solution of Br-silane in anhydrous toluene and kept in a dry environment at room temperature for 3 h. The silicon substrates coated with a self-assembled monolayer of Br-silane (Br-SAM) were then washed with toluene, acetone, and twice with ethanol and DI water, then dried under a stream of nitrogen.[6] Subsequently, the Br-SAM substrates were placed in the reactors under the argon atmosphere and a solution of CTA (66.69 mg, 0.239 mmol), CuBr (6.10 mg, 42.5 μmol), and BiPy (12.99 mg, 83.2 μmol) in deoxygenated anhydrous DMSO (10 mL), previously purged by argon bubbling for 30 min, was added under argon and left to react for 24 h at 30 °C to obtain the CTA-SAM.[10] After the modification, the CTA-SAM substrates were washed with methanol, acetone, and twice with ethanol and DI water, then dried under a stream of nitrogen.

Surface-initiated (SI) RAFT polymerization of HPMA. A flask containing HPMA (3000 mg, 20.95 mmol), CTA (3.37 mg,

12.1 μmol), and AIBN (1.98 mg, 12.1 μmol) sealed with a septum was purged with argon for 1 h in an ice bath. In the meantime, the solvents were also purged with argon individually. Then, 12 mL of the selected composition of water and DMF or 1,4-dioxane solution mixture were transferred to the flask containing the solids. The final mixture was transferred to the reactors containing the CTA-SAM substrates after vigorous stirring to completely dissolve the individual components of the mixture (*Note*: The polymerizations could not be performed in pure water due to the insolubility of AIBN and CTA. Similarly, pure 1,4-dioxane conditions could not be used to carry out the SI-RAFT polymerization of HPMA due to limited solubility of monomer). The polymerization was carried out by placing the sealed reactors with the reaction mixture in a temperature-controlled oil bath at 80 °C for the specified time. The polymerization was quenched by opening the reaction vessels to the atmosphere and rapidly cooling the solution in an ice bath. 200 μL of the quenched reaction mixture were transferred to an NMR tube with 500 μL of deuterated dimethyl sulfoxide (d-DMSO) for NMR measurement of the conversion. The rest of the solution was dialyzed against DI water (membrane molecular weight cut-off 1 kDa), which was regularly renewed for 24 h, and then lyophilized. Afterwards, the solution-born p(HPMA) was characterized by SEC-MALS to obtain the molar mass and dispersity. Substrates coated with the p(HPMA) were rinsed with methanol, acetone and twice washed by ethanol and DI water, then dried under a stream of nitrogen.

Aminolysis of end groups of surface-grafted p(HPMA) for SMFS measurement. To promote the chemical binding between the AFM-tip and the polymer chain-end groups, the latter were converted to thiol *via* aminolysis of the CTA. A flask of anhydrous ethanol and a flask containing hexylamine (20 μL, 0.153 mmol) and TEA (20 μL, 0.143 mmol) were deoxygenated by purging with argon for 10 min.[33] The reaction solution was prepared by adding 5 mL of degassed ethanol into the flask with the amines. Then, the amine solution was transferred to the reactors containing the p(HPMA)-coated substrates at room temperature under argon atmosphere for 3 h. Afterwards, the substrates coated with p(HPMA) brushes bearing thiol end groups were washed with methanol, acetone, and twice with ethanol and DI water, then dried under a stream of nitrogen. The surface-grafted polymer layers were fully characterized by SE and AFM-SMFS.

Characterization

Nuclear magnetic resonance (NMR). Samples were collected for every condition at 0.5 h, 1.0 h, 1.5 h, 2.0 h, 2.5 h, and 3.0 h and measured by ^{1}H-NMR (Bruker Avance III spectrometer operating at 300.13 MHz (^{1}H) in d-DMSO) to determine the monomer conversion.

Spectroscopic ellipsometry (SE). Ellipsometric data were acquired using a J.A. Woollam M-2000X spectroscopic ellipsometer operating in rotating compensator mode in the angle of incidence range 60–70° (with a step of 5°) and spectral range of λ = 250–1000 nm. Data were analysed in the CompleteEASE software package using multilayer models and Cauchy dispersion relation for the p(HPMA) layer.

Single-molecule force spectroscopy (SMFS)

The SMFS measurements were performed using an atomic force microscopy setup microscope (Bruker JPK Nanowizard) working in force spectroscopy mode with gold-coated tips (MikroMasch, HQ:CSC38/Cr–Au, consisting of three cantilevers with a nominal tip radius of 35 nm). The SMFS measurements were carried out in DI water. After mounting the cantilever, calibration was done for the sensitivity and the spring constant. The tip separation from the sample was set to 500 nm and the movement of the force curves was performed with a frequency of 0.5 Hz. The data was analysed in the Data Processing software of Bruker JPK. From the measured curves, the ones with rupture events were selected and were fitted to the worm-like chain (WLC) model to obtain the contour length of the polymer chains (see ESI†).[33]

Size exclusion chromatography equipped with multiple angle laser light scattering (SEC-MALS)

The molar mass distribution of the solution-born p(HPMA) was measured by using a Shimadzu HPLC system equipped with a Superose 6 column, online UV detector (Shimadzu), differential refractive index detector (Wyatt Optilab T-rEX) and multi-angle light scattering (Wyatt Dawn Heleos-II). The mobile phase used for the measurement was 0.3 M sodium acetate buffer (pH 6.5) with 1 g L^{-1} of sodium azide flowing at 0.5 mL min^{-1}, and the specific refractive index increment ($dn{\cdot}dc^{-1}$) of p(HPMA) was taken to be as 0.167.

Dynamic viscosity measurement

Dynamic viscosity was measured using a rotational rheometer ARES G2 (TA Instruments, USA). Shear flow measurements were performed at 23 °C in the range of shear rates from 1 to 10 s^{-1} using cone-plate geometry with a plate diameter of 25 mm and cone angle of 0.1 rad. Additionally, viscosity measurements were attempted at the polymerization temperature of 80 °C but could not be carried out due to solvent evaporation losses in the open measurement chamber.

Results and discussion

In pursuit of SI-RAFT polymerization conditions providing poly(HPMA) brushes of controlled parameters, we investigated the discrepancy between surface and solution polymerization. We focused on the effect of the solvent composition, as this was previously shown by Thang and coworkers to have a critical influence on the propagation rate and attainable control in the conventional solution-based RAFT polymerization of HPMA.[54] We adjust the solution propagation rate by the solvent effects and observe the discrepancy in the molar mass between polymers grown in solution and on the surface. The set of conditions employed for the SI-RAFT polymerization of HPMA differed only in composition of the solvent, which con-

Table 1 Solvent conditions of SI-RAFT polymerization of HPMA[a,b]

Entry	Solvent composition		Designation	k_{app} (min^{-1})
1	DMF 100%	Water 0%	DMF 100%	0.0013
2	DMF 75%	Water 25%	DMF 75%	0.0023
3	DMF 50%	Water 50%	DMF 50%	0.0026
4	DMF 25%	Water 75%	DMF 25%	0.0035
5	1,4-Dioxane 75%	Water 25%	1,4-Dioxane 75%	0.0028
6	1,4-Dioxane 50%	Water 50%	1,4-Dioxane 50%	0.0046
7	1,4-Dioxane 25%	Water 75%	1,4-Dioxane 25%	0.0039

[a] AIBN and CTA are insoluble in pure water. [b] HPMA monomer is only partially soluble in pure 1,4-dioxane.

sisted of mixtures of water and either DMF (polar, aprotic) or 1,4-dioxane (non-polar, aprotic) (see Table 1, pure 1,4-dioxane was not used due to incomplete solubility of the monomer). P(HPMA) was grown simultaneously in solution and on the surface from sites of CTA attachment. Solution-phase RAFT polymerization follows a well-known mechanism,[55,58–60] but on the surface, the process has a slightly different initiation (Scheme 1). In this study, the R-group of the CTA was bonded covalently to the surface (I).

The radicals are initially formed in solution (II) and transfer reversibly to the thiocarbonylthio (S=C–S) moiety of surface-bound CTA, leaving behind a radical in the surface-anchored R-group (II). Subsequently, the surface propagation (III) starts, involving HPMA monomer diffusion to the radical-bearing R-group on the surface. In this way, the surface-grafted and solution-born polymers grow simultaneously (IV) *via* RAFT polymerization.[10] The surface-attached CTA forms a monolayer. While its local concentration on the surface is high, its total amount is very low in comparison with the monomer and initiator concentrations in solution. Because of this, in SI-RAFT it is usually necessary to add "free" soluble CTA in the polymerization mixture in order to attain controlled RAFT polymerization in solution. This free CTA also aids in the exchange of radicals between surface and solution to limit termination, which can be increased on the surface due to the high local concentration of radicals. In the case of HPMA, a methacrylamide monomer, termination could occur by radical mechanisms as well as possibly by chain-end degradation,

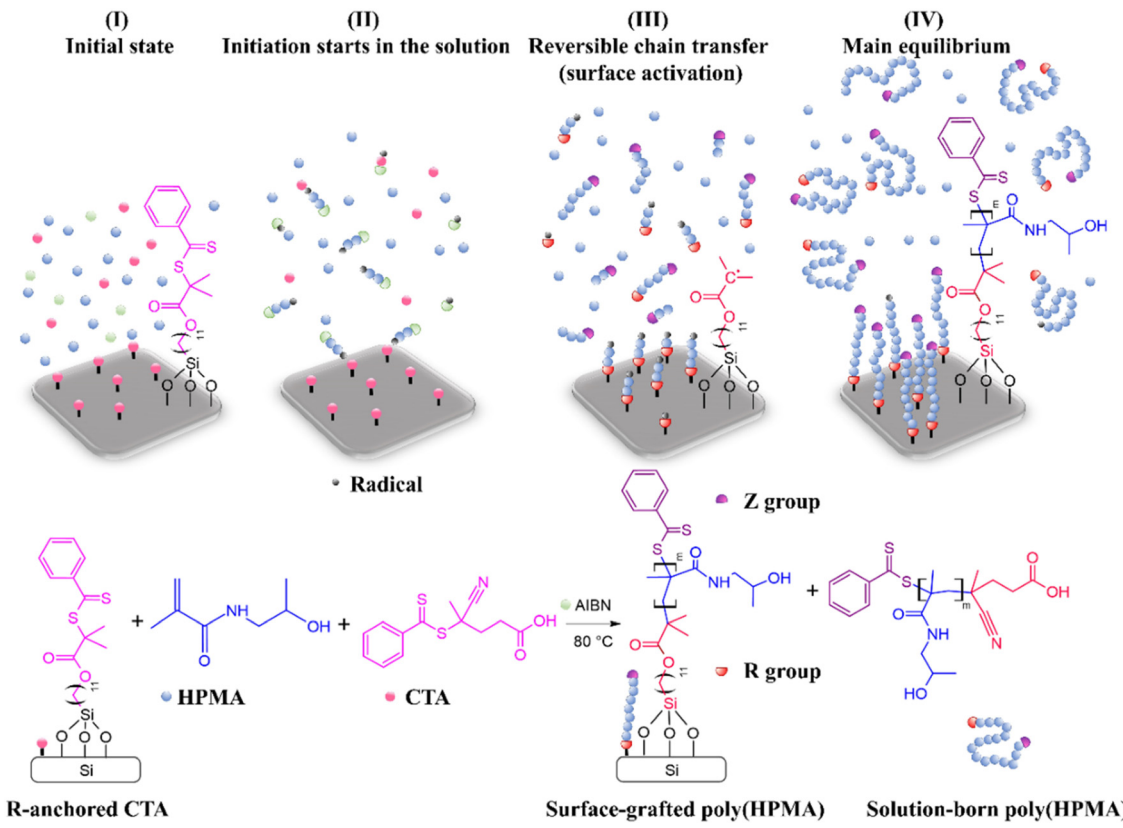

Scheme 1 Illustration and chemical structure of propagation on the surface and in the solution during SI-RAFT polymerization of HPMA.

facilitated by a nucleophilic attack on the thiocarbonyl by the terminal methacrylamide unit.[61–63] Addition of free CTA has also been shown to be beneficial in the synthesis of molecular brushes *via* RAFT using the R-group approach.[64]

Initially, we focused on changing mainly the proticity of the solvent by using mixtures of DMF and water (Table 1, entries 1–4). The molar mass and dispersity of the polymer grown in solution were monitored *via* SEC-MALS (see Fig. S1 and Table S1, ESI†). For each DMF/water composition, the solution polymerization showed a near-linear pseudo-first-order kinetic, pointing to a controlled radical polymerization (see Fig. 1a and b) with a narrow dispersity (see Fig. 1c). In comparison with pure DMF, the conversion increased by 1.6, 1.8 and 2.1 times and the molar mass increased by 1.5, 2.3 and 2.8 times in the solution when the water content changed to 25%, 50% and 75%, respectively (see detailed value at Table S1, ESI†). We performed a linear regression fit of the conversion plots using eqn (S2)† to obtain the apparent propagation rate constant $k_{p,\,app}$. $k_{p,\,app}$ gradually increased with the increase in solvent proticity, *i.e.* higher percentage of water present in the polymerization mixture (Table 1). These results are comparable with Thang's study in that having more water in the solution is beneficial for the control of the RAFT polymerization of HPMA.[54]

Their work also presented temperature-dependent NMR experiments and computational simulation as evidence that in aprotic solvent, the intra- and intermolecular hydrogen bonding between polymer chains and monomer leads to retardation due to hindered fragmentation of the RAFT adduct. Increasing amounts of water in the solution mitigates the retardation. Notably, a control experiment was performed, where no free soluble CTA was added in the polymerization mixture (*i.e.* the only CTA present was the one immobilized on the surface). The obtained polymer demonstrated the expected uncontrolled polymerization process (Fig. S12 and S13, ESI†) as the surface-attached CTA does not affect the solution polymerization, probably owing to its minute amount and limited diffusion.

To analyse the surface-grafted polymers, the course of the polymerization on the surface was monitored by measuring the dry thickness of the polymer layer *via* spectroscopic ellipsometry (see Fig. 2a). As the thickness of the layers increases with time, the surface-grafted polymer chains appear to be growing during the 3 h of polymerization, suggesting that termination reactions are not significant on the surface. In the control experiment carried out without addition of free CTA in the solution, the thickness growth slows down and stops after 2 h (see Fig. S12, ESI†). This points to termination due to gradual loss of the CTA end groups and emphasizes the importance of the added free CTA to enable controlled SI-RAFT.

Interestingly, the thickness of the controlled SI-RAFT did not follow the trend observed for the conversion and molar mass in solution. Indeed, the thicknesses obtained after 180 min under conditions DMF 75% (32.2 nm) and DMF 50% (25.6 nm) were 1.3 and 1.1 times higher than for DMF 100% (24.2 nm), respectively (see Table S3, ESI†). However, at the highest water content DMF 25% (14.8 nm) the thickness was thinner than that of DMF 100% by 0.6 times. This indicates that there is less polymer formed on the surface at the highest solvent water content than in pure DMF, in spite of the enhanced propagation rate observed in solution.

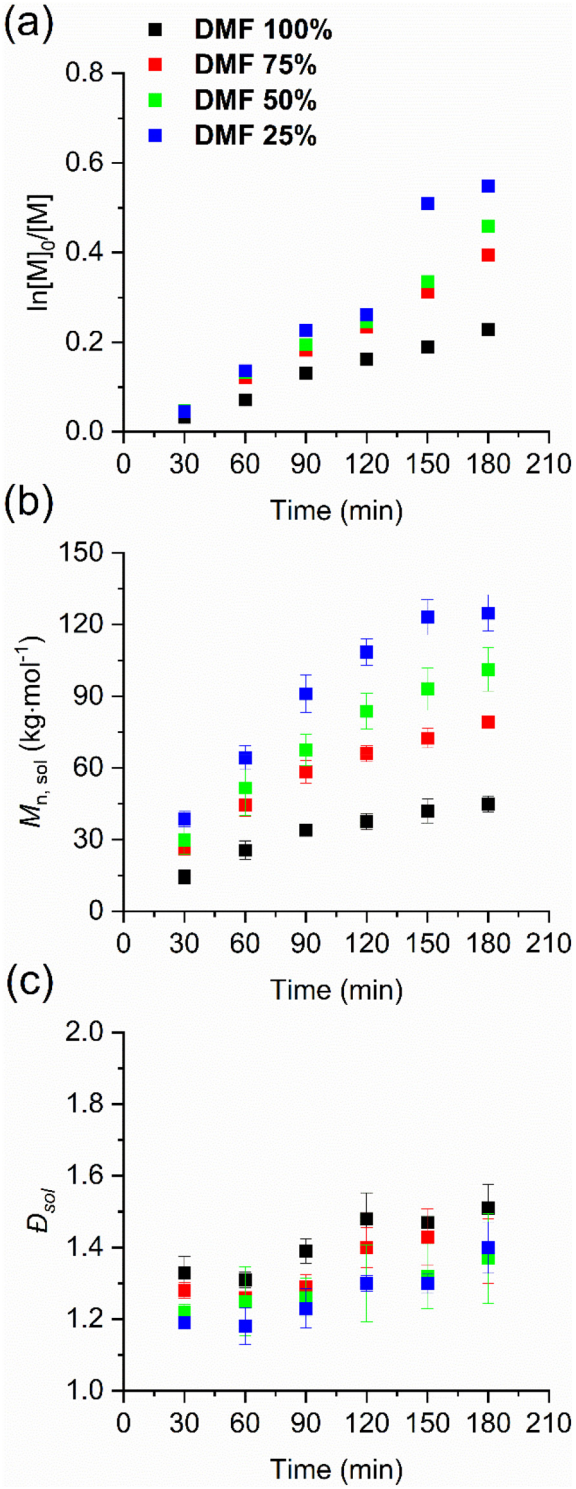

Fig. 1 Kinetic plots of the solution-born p(HPMA) *via* SI-RAFT polymerization in the DMF/water system: (a) conversion, (b) $M_{n,\,sol}$, and (c) dispersity against time. Individual values are reported in Table S1, ESI.†

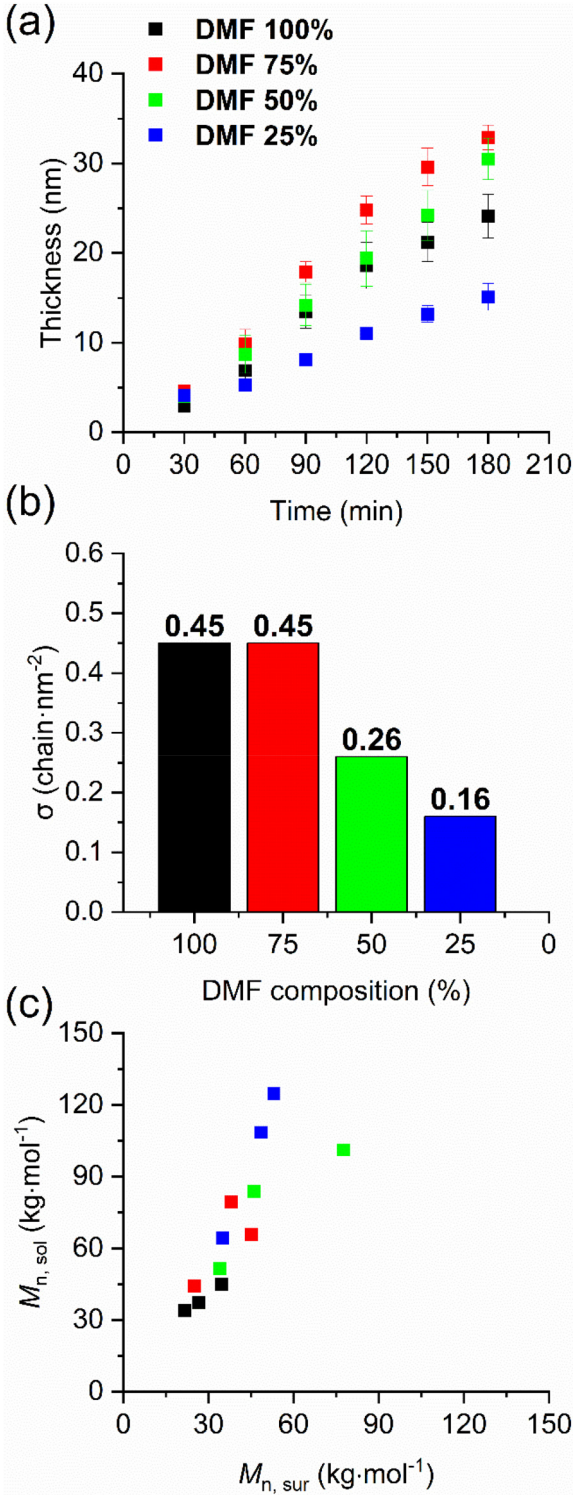

Fig. 2 Kinetic plots of the surface-grafted p(HPMA) *via* SI-RAFT polymerization in the DMF/water system: (a) dry thickness against time, (b) grafting density against solvent composition, and (c) the relation between $M_{n, sol}$ and $M_{n, sur}$. Individual values are reported in Table S3, ESI.†

To characterize the molar mass of the surface-grafted polymers, we employed SMFS to obtain the contour length distribution from each solvent condition. The force–distance curves showing rupture events during retraction of the AFM tips were fitted according to eqn (S3)† to obtain the contour length, l_c for each sampled polymer chain (see Fig. S3, ESI,† for a representative force curve fit) and calculate the number-average molar mass, $M_{n, sur}$ (the obtained molar mass distributions are presented in Fig. S4–S7, ESI†).[10,33,65] Increasing water content in the polymerization mixture leads to increased $M_{n, sur}$, in agreement with the faster propagation observed in solution (see Table S3, ESI†), however, $M_{n, sur}$ showed a decreased propagation rate at condition DMF 25% compared to DMF 50%. This could be caused by mass transfer limitations: the propagation rate increases both in solution and on the surface, but the high local concentration of growing polymer chains on the surface rapidly depletes the monomer concentration in the interface region. At increasing propagation rates, the diffusion of reactants to the surface presumably creates a bottleneck for the continued growth of polymer on the surface, which lags the solution propagation when the solvent proticity increases. Moreover, increasing water content in the polymerization leads to increased conversion in solution, which could be associated with an increase in solution viscosity.

We hypothesized that an increase in viscosity could further limit mass transfer to the surface, as the rate of diffusion has an inverse dependence with viscosity, which poses a frictional resistance to diffusion. To assess this possibility, we measured the dynamic viscosity of the DMF/water polymerization system. Fig. 3 reports the shear rate dependence of the dynamic viscosity in various p(HPMA) DMF/water solutions at various polymerization times. We observed an increase in dynamic viscosity with increased reaction time and water content progressively, suggesting that the higher conversion and associated larger viscosity could play a role in increased mass transfer limitations at high water contents. Moreover, the shear-thinning behaviour of the solutions at high DMF/low water content may indicate interactions such as hydrogen bonding between the polymer, monomer, and solvent molecules. At higher

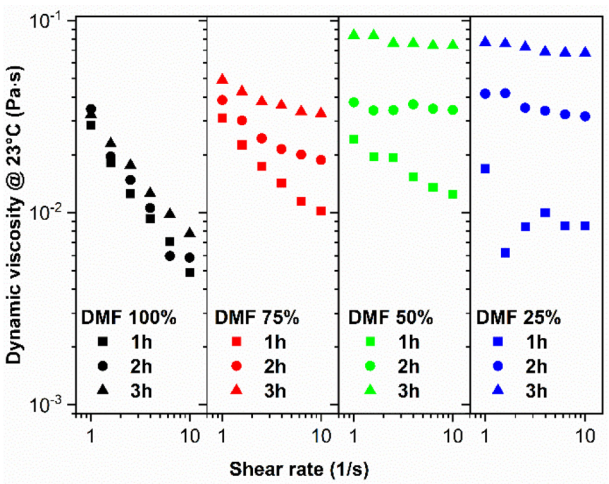

Fig. 3 Shear rate dependence of dynamic viscosity in various p(HPMA) DMF/water solutions at 23 °C.

water contents, these interactions are disrupted as observed by a shift in the dependence of dynamic viscosity on shear rate, when the shear-thinning behaviour (DMF 100% and DMF 75%) changes to a Newtonian fluid behaviour (DMF 50% and DMF 25%).[66] This observation aligns with the conclusions from Thang and co-workers regarding solution RAFT polymerization of HPMA, where the disruption of these hydrogen-bonding interactions was found to be the primary mechanism by which water alleviates retardation and promotes faster propagation. Nevertheless, this does not explain the paradoxical tendency of the thickness, which reaches a maximum for condition DMF 75%, but decreases for conditions DMF 50% and DMF 25% in spite of the faster propagation in solution.

The amount of polymer formed on the surface is determined not only by $M_{n,\,sur}$ but also by the number of chains on a given surface area, *i.e.* the polymer grafting density.[20,21] We calculated the grafting density in each condition by plotting $M_{n,\,sur}$ *vs.* the dry thickness and performed a linear regression fit using eqn (S6) (see Fig. S11a, ESI†).[41] Interestingly, conditions DMF 100% and DMF 75% provided a comparable grafting density of 0.45 chain per nm^2, but increasing water content led to lower grafting densities of 0.26 chain per nm^2 and 0.16 chain per nm^2 for DMF 50% and DMF 25%, respectively (see Fig. 2b). For the control experiment without free CTA in the polymerization mixture, SMFS measurements were attempted but did not yield reliable results, probably due to loss of the polymer CTA end groups during SI-RAFT polymerization (see Fig. S14, ESI†). Besides its influence on the propagation rate, increased solvent proticity may also affect the polymerization on the surface by a distinct mechanism. By disrupting polymer–polymer and polymer–monomer hydrogen bonding interactions on the surface, increased water content promotes solvent interactions with the grafted polymer. Accordingly, the grafted p(HPMA) chains would swell and stretch more due to increased uptake of solvent molecules, creating a larger steric hindrance with increasing water content (Scheme S1, ESI†). This limits the ability of the p(HPMA) chains to grow in close proximity to each other, lowering the grafting density. On the other hand, in pure DMF the p(HPMA) chains would tend to form hydrogen bonds between the side chains and adopt a more compact conformation. Thus, the polymer chains can grow closely together and reach a high grafting density. The lower grafting density in conditions DMF 50% and DMF 25% explains the decreasing thickness in spite of the faster polymerization kinetics in solution.

To further study the solvent effects on the SI-RAFT of HPMA, we used mixtures of 1,4-dioxane and water at varying ratios (Table 1, entries 5–7). As 1,4-dioxane is less polar than DMF, we expect a clear effect of the solvent mixture composition on the grafting density. The conversion plot showed a near-linear pseudo-first order kinetic (see Fig. 4a and detailed values at Table S2, ESI†). However, the molar mass reaches a plateau after about 120 minutes for 1,4-dioxane 75% and 1,4-dioxane 50% (see Fig. 4b and detailed values at Table S2, ESI†), with slightly increased dispersity in comparison to the DMF/water systems (see Fig. 4c). Compared with the DMF/water system, we observed that the 1,4-dioxane/water system had an overall faster propagation rate but a wider dispersity. Looking at the thickness of the concomitantly formed polymer

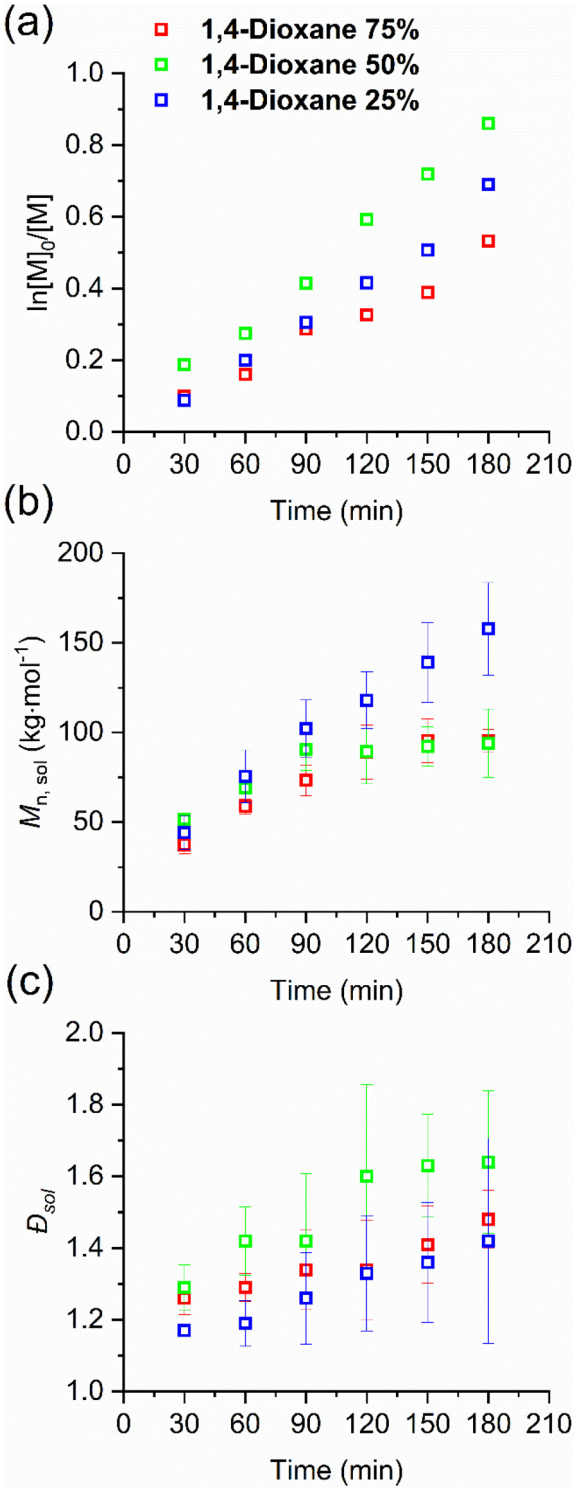

Fig. 4 Kinetic plots of the solution-born p(HPMA) *via* SI-RAFT polymerization in the 1,4-dioxane/water system: (a) conversion, (b) $M_{n,\,sol}$, and (c) dispersity against time. Individual values are reported in Table S2, ESI.†

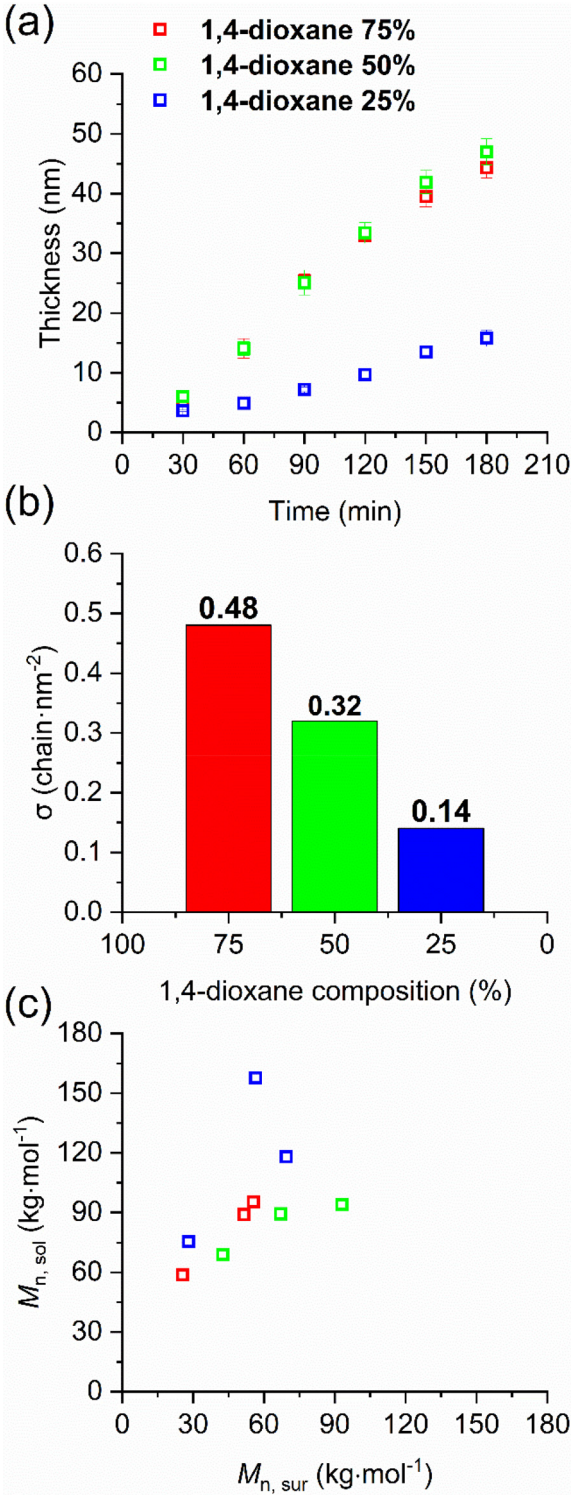

Fig. 5 Kinetic plots of the surface-grafted p(HPMA) *via* SI-RAFT polymerization in the 1,4-dioxane/water system: (a) dry thickness against time, (b) grafting density against solvent composition, and (c) the relation between $M_{n,\,sol}$ and $M_{n,\,sur}$. Individual values are reported in Table S4, ESI.†

layers (see Fig. 5a), we found that 1,4-dioxane 75% and 1,4-dioxane 50% reached a higher thickness than those of DMF/water mixtures. Importantly, increasing the water content to 75% (1,4-dioxane 25%) led to a much lower thickness, comparable to DMF 25%. This agrees with the observations in the DMF mixtures, but in the 1,4-dioxane/water system the difference in thickness was even more marked. To assess the grafting density, we employ SMFS to determine the $M_{n,\,sur}$ (the obtained molar mass distributions are presented in Fig. S8–S10 and detailed values at Table S4, ESI†). We also plotted $M_{n,\,sur}$ *vs.* the dry thickness and performed a linear regression fit using eqn (S6)† to obtain the grafting density for 1,4-dioxane/water systems (see Fig. S11b, ESI†). The grafting density of the p(HPMA) layer in 1,4-dioxane/water systems greatly decreased with increasing content of water in the polymerization mixture, in agreement with the results obtained for the DMF/water system (see Fig. 5b and Table S4, ESI†), supporting our hypothesis.

Finally, we compared $M_{n,\,sol}$ and $M_{n,\,sur}$ in each condition, starting with the DMF/water system, and verified their discrepancy. In Fig. 2c, the position of each point represents $M_{n,\,sol}$ and $M_{n,\,sur}$ at a given polymerization for a given solvent condition. While both $M_{n,\,sol}$ and $M_{n,\,sur}$ increased with increasing the water percentage, the absolute values show a growing discrepancy, which is seen by $M_{n,\,sol}$ increasing faster than $M_{n,\,sur}$. At the highest water content (condition DMF 25%) the largest discrepancy between the $M_{n,\,sol}$ and $M_{n,\,sur}$ was observed in comparison with the other three conditions, with the ratio $M_{n,\,sol}/M_{n,\,sur}$ reaching as high as 2.4. Similarly, in the case of ATRP polymerizations the enhanced rate of propagation was found to play an important role in the discrepancy between the M_n of the polymer obtained in solution and on the surface.[40] Solvent polarity and water content are critical in ATRP, as they shift the value of K_{ATRP}. The enhanced propagation observed in solution RAFT with increasing water content is caused the facilitated fragmentation of the RAFT adduct through hydrogen bonding with the solvent. Thus, both in ATRP and RAFT polymerization, the mechanism is of central importance for the effect of the solvent and for the observed differences in M_n between surface and solution. The comparison reported in our study experimentally demonstrated that higher propagation rate led to a larger discrepancy of molar masses between the surface-grafted and solution-born polymers. We hypothesized the larger discrepancy between the surface-grafted and the solution-born polymers was induced by the mass transfer limitation which accompanies the higher solution propagation rate. The increased viscosity caused by higher conversion and $M_{n,\,sol}$ for the highest water content slows down diffusion to the surface further limiting surface propagation and causing it to lag propagation in solution. Similarly as for DMF/water mixtures, also in the case of the 1,4-dioxane/water systems the largest discrepancy between the molar masses of the polymer formed in solution and on the surface was observed for the highest water content, *i.e.* condition 1,4-dioxane 25%. This can be visualized in Fig. 5c by the larger $M_{n,\,sol}$ in comparison to $M_{n,\,sur}$ for each point for that condition.

It is interesting to compare these results with our previous observations on the SI-RAFT polymerization of HPMA in methanol using a low-temperature initiator.[10] At 45 °C and

with a low-temperature initiator, the polymerization proceeded much more slowly. After 24 h of reaction, the molar mass of the solution-grown polymer $M_{n,\,sol}$ reached 44.6 kg mol^{-1} and the thickness of the grafted p(HPMA) layer was 13.5 nm with $M_{n,\,sur}$ reached 49 kg mol^{-1}. Notably and in contrast to the results of our current study, the molar masses of the p(HPMA) formed in solution and grafted from the surface were found to be comparable. This can be explained by the much slower polymerization kinetics, which negated the effect of mass transport limitations between surface and solution. Furthermore, the grafting density of the p(HPMA) brushes obtained under those conditions was 0.18 chain per nm^2, which is comparable to the polymer layers prepared in the current study in solvent mixtures with 75% of water, both of DMF and 1,4-dioxane. This is consistent with the methanol being able to solvate the HPMA monomer and surface-grafted p(HPMA) thanks to its hydrogen bonding capacity. Taken together, these results confirm the decisive effect of polymerization kinetics on the discrepancy between the molar masses of the polymer formed in solution and grafted from the surface. They also support the role of the solvent in determining the grafting density of the polymer grafted during SI-RAFT.

Conclusions

In conclusion, enhancing the solution propagation rate by having a higher water content in the solvent leads to a larger discrepancy between the molar masses of the polymer grown on the surface and in solution. Importantly, we discover that the proticity and polarity of the solvent also directly affect the achievable grafting density of p(HPMA), which could be elucidated through the use of SMFS. This is probably due to the chains on the surface adopting a more extended conformation as the polymer–polymer interactions are reduced. As a consequence, in spite of the increased propagation rate, the thickness of the p(HPMA) layer is decreased under higher solvent proticity and polarity. Therefore, an optimized synthesis of p(HPMA) brushes *via* the SI-RAFT polymerization may be achieved in an aprotic solvent, under the precondition that a well-controlled CRP in the solution is maintained, in this case through the addition of a small fraction of water. Importantly, while in solution RAFT polymerization high conversions are generally targeted, the associated increase in viscosity contributes to mass transfer limitations in the surface polymerization and a discrepancy between solution and surface polymerization conditions. The present study highlights the importance of the solvent effects on SI-RAFT polymerization and how they act by multiple mechanisms simultaneously, exerting a complex influence on the polymer grafting process. It must be noted that the solvent effects discussed in the present report are specific to the HPMA monomer and its SI-RAFT polymerization in aprotic and water-containing solvent mixtures. Thus, further studies on other monomers and their interactions with different solvents during SI-RAFT and other SI-polymerizations present an interesting potential research direction to tune the molar mass and the grafting density of surface-grafted polymers. Such considerations are especially important for coating applications where the grafting density plays a decisive role, such as biomaterials.

Author contributions

Y. W. – conceptualization, investigation, methodology, formal analysis, writing – original draft, writing – review & editing; A. K., Y. H., and H. B. – investigation, methodology, formal analysis, writing – review & editing; A. d. l. S. P. and O. P.-G. – conceptualization, supervision, writing – review & editing, funding acquisition.

Conflicts of interest

There are no conflicts to declare.

Acknowledgements

The authors acknowledge the support from the Czech Science Foundation (project no. 22-02836S). A. d. l. S. P. acknowledges funding from the Czech Science Foundation (project no. 22-27329S). The work was supported by the project "National Institute for Cancer Research (Programme EXCELES, ID project no. LX22NPO5102) – funded by the European Union – Next Generation EU". The experimental work of SMFS was performed during the implementation of the project Building-up Centre for advanced materials application of the Slovak Academy of Sciences, ITMS project code 313021T081 supported by the Integrated Infrastructure Operational Programme funded by ERDFW.

References

1 V. Šubr, L. Kostka, J. Strohalm, T. Etrych and K. Ulbrich, *Macromolecules*, 2013, **46**, 2100–2108.
2 J. Kopecek, P. Kopeckova, T. Minko and Z. Lu, *Eur. J. Pharm. Biopharm.*, 2000, **50**, 61–81.
3 O. Hovorka, T. Etrych, V. Šubr, J. Strohalm, K. Ulbrich and B. Říhová, *J. Drug Targeting*, 2006, **14**, 391–403.
4 P. Chytil, T. Etrych, J. Kříž, V. Šubr and K. Ulbrich, *Eur. J. Pharm. Sci.*, 2010, **41**, 473–482.
5 M. Vorobii, A. de los Santos Pereira, O. Pop-Georgievski, N. Y. Kostina, C. Rodriguez-Emmenegger and V. Percec, *Polym. Chem.*, 2015, **6**, 4210–4220.
6 A. de los Santos Pereira, S. Sheikh, C. Blaszykowski, O. Pop-Georgievski, K. Fedorov, M. Thompson and C. Rodriguez-Emmenegger, *Biomacromolecules*, 2016, **17**, 1179–1185.
7 E. Roeven, A. R. Kuzmyn, L. Scheres, J. Baggerman, M. M. J. Smulders and H. Zuilhof, *Langmuir*, 2020, **36**, 10187–10199.

8 P. Alves, L. C. Gomes, M. Vorobii, C. Rodriguez-Emmenegger and F. J. Mergulhão, *Colloids Surf., B*, 2020, **19**, 110976.
9 Z. Riedelová, A. d. l. S. Pereira, J. Svoboda, O. Pop-Georgievski, P. L. Májek, K. Pečánková, F. Dyčka, C. Rodriguez-Emmenegger and T. Riedel, *Macromol. Biosci.*, 2022, **22**, 2200247.
10 Y. Wang, A. Kálosi, Y. Halahovets, I. Romanenko, J. Slabý, J. Homola, J. Svoboda, A. de los Santos Pereira and O. Pop-Georgievski, *Polym. Chem.*, 2022, **13**, 3815–3826.
11 R. Wang, Q. Wei, W. Sheng, B. Yu, F. Zhou and B. Li, *Angew. Chem., Int. Ed.*, 2023, **62**, e202219312.
12 M. Badoux, M. Billing and H.-A. Klok, *Polym. Chem.*, 2019, **10**, 2925–2951.
13 O. Roling, A. Mardyukov, J. A. Krings, A. Studer and B. J. Ravoo, *Macromolecules*, 2014, **47**, 2411–2419.
14 W. Wei, A. Balamurugan, J. H. Dwyer and P. Gopalan, *ACS Macro Lett.*, 2018, **7**, 100–104.
15 A. C. Schmidt, H. Turgut, D. Le, A. Beloqui and G. Delaittre, *Polym. Chem.*, 2019, **11**, 593–604.
16 S. Yamago, Y. Yahata, K. Nakanishi, S. Konishi, E. Kayahara, A. Nomura, A. Goto and Y. Tsujii, *Macromolecules*, 2013, **46**, 6777–6785.
17 A. Layadi, B. Kessel, W. Yan, M. Romio, N. D. Spencer, M. Zenobi-Wong, K. Matyjaszewski and E. M. Benetti, *J. Am. Chem. Soc.*, 2020, **142**, 3158–3164.
18 R. Sivkova, J. Svoboda, J. Pánek, D. Appelhans and O. Pop-Georgievski, *Prog. Org. Coat.*, 2023, **178**, 107447.
19 Y. Ko, V. K. Truong, S. Y. Woo, M. D. Dickey, L. Hsiao and J. Genzer, *Biomacromolecules*, 2022, **23**, 424–430.
20 S. Yamamoto, M. Ejaz, Y. Tsujii, M. Matsumoto and T. Fukada, *Macromolecules*, 2000, **33**, 5602–5607.
21 S. Yamamoto, M. Ejaz, Y. Tsujii and T. Fukada, *Macromolecules*, 2000, **33**, 5608–5612.
22 C. Rodriguez-Emmenegger, B. V. K. J. Schmidt, Z. Sedlakova, V. Šubr, A. B. Alles, E. Brynda and C. Barner-Kowollik, *Macromol. Rapid Commun.*, 2011, **32**, 958–965.
23 M. Zamfir, C. Rodriguez-Emmenegger, S. Bauer, L. Barner, A. Rosenhahn and C. Barner-Kowollik, *J. Mater. Chem. B*, 2013, **1**, 6027–6034.
24 X. Xu, X. Huang, Y. Chang, Y. Yu, J. Zhao, N. Isahak, J. Teng, R. Qiao, H. Peng, C. Zhao, T. P. Davis, C. Fu and A. K. Whittaker, *Biomacromolecules*, 2021, **22**, 330–339.
25 A. R. Kuzmyn, A. T. Nguyen, L. W. Teunissen, H. Zuilhof and J. Baggerman, *Langmuir*, 2020, **36**, 4439–4446.
26 A. R. Kuzmyn, M. van Galen, B. van Lagen and H. Zuilhof, *Polym. Chem.*, 2023, **14**, 3357–3363.
27 J. Yuan, X. Huang, P. Li, L. Li and J. Shen, *Polym. Chem.*, 2013, **4**, 5074–5085.
28 M. K. Cho, H. J. Seo, J. H. Lee, W. K. Cho and K. Son, *Polym. Chem.*, 2021, **12**, 7023–7030.
29 Y. Zhao and S. Perrier, in *Controlled Radical Polymerization at and from Solid Surfaces*, ed. P. Vana, Springer, Cham: Switzerland, 2015, vol. 270, pp. 77–106.
30 C. Chen, F. Richter, C. Guerrero-Sanchez, A. Traeger, U. S. Schubert, A. Feng and S. H. Thang, *ACS Macro Lett.*, 2020, **9**, 260–265.
31 M. Li, M. Fromel, D. Ranaweera, S. Rocha, C. Boyer and C. W. Pester, *ACS Macro Lett.*, 2019, **8**, 374–380.
32 A. Halperin, *Langmuir*, 1999, **15**, 2525–2533.
33 T. Tischer, R. Gralla-Koser, V. Trouillet, L. Barner, C. Barner-Kowollik and C. Lee-Thedieck, *ACS Macro Lett.*, 2016, **5**, 498–503.
34 L. Michalek, L. Barner and C. Barner-Kowollik, *Adv. Mater.*, 2018, **30**, 1706321.
35 D. Goodman, J. N. Kizhakkedathu and D. E. Brooks, *Langmuir*, 2004, **20**, 6238–6245.
36 M. Fromel, E. M. Benetti and C. W. Pester, *ACS Macro Lett.*, 2022, **11**, 415–421.
37 J. O. Zoppe, N. C. Ataman, P. Mocny, J. Wang, J. Moraes and H.-A. Klok, *Chem. Rev.*, 2017, **117**, 1105–1318.
38 E. Turan, S. Demirci and T. Caykara, *Thin Solid Films*, 2010, **518**, 5950–5954.
39 E. H. Min, S. R. S. Ting, L. Billon and M. H. Stenzel, *J. Polym. Sci., Part A: Polym. Chem.*, 2010, **48**, 3440–3455.
40 C. Kang, R. Crockett and N. D. Spencer, *Polym. Chem.*, 2016, **7**, 302–309.
41 R. R. Patil, S. Turgman-Cohen, J. Šrogl, D. Kiserow and J. Genzer, *Langmuir*, 2015, **31**, 2372–2381.
42 A. Al-Baradi, M. R. Tomlinson, Z. J. Zhang and M. Geoghegan, *Polym. Chem.*, 2015, **67**, 111–117.
43 A. R. Kuzmyn, T. G. Ypma and H. Zuihof, *Langmuir*, 2024, **40**, 3354–3359.
44 S. Yamamoto, Y. Tsujii and T. Fukuda, *Macromolecules*, 2000, **33**, 5995–5998.
45 S. Al-Maawali, J. E. Bemis, B. B. Akhremitchev, R. Leecharoen, B. G. Janesko and G. C. Walker, *J. Phys. Chem. B*, 2001, **105**, 3965–3971.
46 S. S. Sheiko, M. d. Silva, D. Shirvaniants, S. LaRue, S. Prokhorova, M. Moeller, K. Beers and K. Matyaszewski, *J. Am. Chem. Soc.*, 2003, **125**, 6725–6728.
47 S. S. Sheiko, O. V. Borisov, S. A. Prokhorova and M. Möller, *Eur. Phys. J. E*, 2004, **13**, 125–131.
48 S. S. Sheiko, in *New Developments in Polymer Analytics II*, ed. M. Schmidt, Springer Berlin Heidelberg, 2000, vol. 151, pp. 61–174.
49 G. M. Scheutz, J. I. Bowman, S. Mondal, J. Y. Rho, J. B. Garrison, J. Korpanty, N. C. Gianneschi and B. S. Sumerlin, *ACS Macro Lett.*, 2023, **12**, 454–461.
50 Y. Terayama, M. Kikuchi, M. Kobayashi and A. Takahara, *Macromolecules*, 2011, **44**, 104–111.
51 M. Kobayashi, H. Yamaguchi, Y. Terayama, Z. Wang, K. Ishihara, M. Hino and A. Takahara, *Macromol. Symp.*, 2009, **279**, 79–87.
52 W. A. Braunecker, N. V. Tsarevsky, A. Gennaro and K. Matyjaszewski, *Macromolecules*, 2009, **42**, 6348–6360.
53 N. V. Tsarevsky, T. Pintauer and K. Matyjaszewski, *Macromolecules*, 2024, **37**, 9768–9778.
54 X. Pan, F. Zhang, B. Choi, Y. Luo, X. Guo, A. Feng and S. H. Thang, *Eur. Polym. J.*, 2019, **115**, 166–172.
55 S. Pirrier, *Macromolecules*, 2017, **50**, 7433–7447.

56 C. Rodriguez-Emmenegger, S. Janel, A. de los Santos Pereira, M. Bruns and F. Lafont, *Polym. Chem.*, 2015, **6**, 5740–5751.
57 K. Ulbrich, V. Šubr, J. Strohalm, D. Plocová, M. Jelínková and B. Říhová, *J. Controlled Release*, 2000, **64**, 63–70.
58 O. R. Courtney, S. M. Clouthier, S. Perrier, J. Tanaka and W. You, *ACS Macro Lett.*, 2023, **12**, 1306–1310.
59 D. K. Schneiderman, J. M. Ting, A. A. Purchel, R. Miranda Jr., M. W. Tirrell, T. M. Reineke and S. J. Rowan, *ACS Macro Lett.*, 2018, **7**, 406–411.
60 T. Nwoko, K. Nguyen, N. K. Saha, C. Barner-Kowollik and D. Konkolewicz, *Polym. Chem.*, 2024, **15**, 1052–1061.
61 B. A. Abel and C. L. McCormick, *Macromolecules*, 2016, **49**, 465–474.
62 M. S. Donovan, A. B. Lowe, B. S. Sumerlin and C. L. McCormick, *Macromolecules*, 2002, **35**, 4123–4132.
63 M. S. Donovan, T. A. Sanford, A. B. Lowe, B. S. Sumerlin, Y. Mitsukami and C. L. McCormick, *Macromolecules*, 2002, **35**, 4570–4572.
64 Z. Zheng, J. Ling and A. H. E. Müller, *Macromol. Rapid Commun.*, 2014, **35**, 234–241.
65 J. McClements and V. Koutsos, *ACS Macro Lett.*, 2020, **9**, 152–157.
66 R. G. Larson, *The structure and rheology of complex fluids*, Oxford University Press New York, New York, 1999.